Journal of Science: Advanced Materials and Devices 4 (2019) 370–375

Contents lists available at ScienceDirect

Journal of Science: Advanced Materials and Devices

journal homepage: www.elsevier.com/locate/jsamd

Original Article

Effect of crystallization temperature on energy-storage density and efficiency of lead-free $Bi_{0.5}(Na_{0.8}K_{0.2})_{0.5}TiO_3$ thin films prepared by sol–gel method

Nguyen Dang Co [a], Le Viet Cuong [a], Bui Dinh Tu [a], Pham Duc Thang [a], Luong Xuan Dien [b], Vu Ngoc Hung [c], Ngo Duc Quan [c, d, *]

[a] Faculty of Engineering Physics and Nanotechnology, VNU-University of Engineering and Technology, 144 Xuan Thuy Road, Cau Giay District, Hanoi, 100000, Viet Nam
[b] School of Chemical Engineering, Hanoi University of Science and Technology, No.1 Dai Co Viet, Hanoi, 100000, Viet Nam
[c] International Institute for Materials Science, Hanoi University of Science and Technology, No.1 Dai Co Viet, Hanoi, 100000, Viet Nam
[d] School of Engineering Physics, Hanoi University of Science and Technology, No.1 Dai Co Viet, Hanoi, 100000, Viet Nam

ARTICLE INFO

Article history:
Received 18 February 2019
Received in revised form
24 April 2019
Accepted 25 April 2019
Available online 30 April 2019

Keywords:
Energy-storage
Ferroelectric
Sol–gel
Film
Lead-free

ABSTRACT

Lead-free $Bi_{0.5}(Na_{0.80}K_{0.20})_{0.5}TiO_3$ (BNKT) ferroelectric films were synthesized on Pt/Ti/SiO_2/Si substrates via the chemical solution deposition. The influence of the crystallization temperature on the microstructures, the ferroelectric and energy-storage properties of the films was investigated in detail. The results showed that the BNKT films have reached the well crystallized state in the single-phase perovskite structure at 700 °C. Ferroelectric and energy-storage properties of the films were significantly enhanced by increasing the crystallization temperature. The remnant polarization ($2P_r$) and maximum polarization ($2P_m$) reached the highest values of 18.4 μC/cm^2 and 61.2 μC/cm^2, respectively, under an applied electric field of 300 kV/cm. Thanks to the strong enhancement in $2P_m$ and the large P_{max} - P_r value, the highest energy-storage density (J_{reco}) and efficiency of 2.3 J/cm^3 and 58.2%, respectively, were obtained. These results indicate that the BNKT films have application potentials in advanced capacitors.

1. Introduction

Ferroelectric materials have played an important role in modern science and technology with different electronic applications. Ferroelectric materials can be used as capacitors with tunable capacitance, thanks to their nonlinear nature, as ferroelectric RAM for computers, RFID cards due to their memory function, *etc*. Also, ferroelectric materials simultaneously exhibit piezoelectric and pyroelectric properties. These combined properties make ferroelectric capacitors very useful for sensor applications, such as: fire sensors, sonar sensors, vibration sensors in medical ultrasound machines, high-quality infrared cameras, and even in fuel injectors on diesel engines [1]. Traditional ferroelectric materials, based on lead as $PbZr_xTi_{1-x}O_3$ (PZT), have attracted particular attention due to their excellent piezoelectric properties [2]. But, because of containing the toxic volatile metal element (Pb), this material system likely causes negative effects on human health and the environment. Therefore, researches on environment-friendly lead-free ferroelectric materials to replace Pb-based ones are necessary and the interesting trends in the present development of ferroelectric materials. Among the potential candidates, the $Bi_{0.5}(Na_{0.80}K_{0.20})_{0.5}TiO_3$ (BNT, BKT and (BNKT) compounds with a certain content range show the morphotropic phase boundary (MPB), where tetragonal and rhombohedral symmetries coexist. However, the concentration range of BKT in the materials, at which the MPB region exists, remains controversial. Jones *et al.* reported that BNKT with x from 0.50 to 0.60 possesses only a rhombohedral symmetry (*R3m*), no the trace of MPB was observed [3]. Kreisel *et al.* also obtained a similar result when studying BNKT between $x = 0.50$ and 0.80 [4]. But Sasaki *et al.* when investigating the $Bi_{0.5}$ $(Na_{1-x}K_x)_{0.5}TiO_3$ system, observed a biphasic range in the neighborhood of the composition $x = 0.16–0.20$ [5], while Elkechai *et al.* found the MPB region in the range between $x = 0.08$ and 0.30 [6]. The variation the mentioned works may be stemmed from different reaction conditions. It was

* Corresponding author. International Institute for Materials Science, Hanoi University of Science and Technology, No.1 Dai Co Viet, Hanoi, 100000, Viet Nam.
E-mail address: quan.ngoduc@hust.edu.vn (N.D. Quan).
Peer review under responsibility of Vietnam National University, Hanoi.

https://doi.org/10.1016/j.jsamd.2019.04.008

believed that in the MPB regions, materials reveal a significant improvement in the electromechanical properties [2]. To specify, Yuji *et al.* reported that BNKT possesses the best electromechanical properties at the composition $x = 0.2$ (MPB) [7] with the $2P$ value of 76 μC/cm^2, the piezoelectric coefficient d_{33} of 167 pC/N, and the electromechanical coupling coefficient k_{33} of 0.56 [8]. In another work, the $2Pr$ and d_{33} coefficients for the BNKT samples with $x = 0.2$ reached their highest values of 80 μC/cm^2 and 134 pC/N, respectively. These enhancements can be related to the local distortions of the rhombohedral and tetragonal structures [9]. Recently, the majority of studies on the BNKT materials have been focused to enhance their energy-storage density (J_{reco}) as well as energy-storage efficiency (η) for the application in pulsed or intermittent power devices with rapid discharge ability [10,11]. It is indicated that there are two reasonable ways to improve the energy-storage density. The first one is to increase the value of the break-down strength (BDS). Oxygen vacancies and defect dipoles are generated thanks to the acceptor substitution. They could create an intrinsic restoring force, hence causing a decline in P_r [12,13]. Besides, oxygen vacancies act as trap sites, causing electron trap levels to become deeper, followed by an improvement of the BDS [14]; The other is to enlarge the difference between P_{max} and P_r. Substituting large atoms at small atom sites will make the lattice constant to become larger [15] and cause compressive stress in the local area. According to the Landau-Ginsburg-Devonshire's theory, the compressive stress may make the Gibbs free energy flat [16] and then reduce the ferroelectric domain reversal barrier, thereby enhancing the value of P_{max}.

In recent studies, we have reported the effect of the processing conditions, such as annealing time [17] or film thickness [18] on the ferroelectric and energy-storage properties of BNKT films. Then, the ferroelectric properties and energy storage density were found significantly enhanced thanks to the design of the heterolayered structures between PLZT and BNKT films [19]. In the present study, we fabricated lead-free $Bi_{0.5}(Na_{0.8}K_{0.2})_{0.5}TiO_3$ (denoted as BNKT) films via a sol–gel method on Pt/Ti/SiO_2/Si substrates and investigated the physical properties of the BNKT films annealed at different temperatures (600, 650, 700 and 750 °C) for 60 min in air. We found that the optimal crystallization temperature is 700 °C. At this, the remanent ($2P_r$) and maximum polarization ($2P_m$) reach their highest values of 18.4 μC/cm^2 and 61.2 μC/cm^2, respectively. The highest energy-storage density (J_{reco}) and efficiency get the values of 2.3 J/cm^3 and 58.2%, respectively.

2. Experimental

The lead-free $Bi_{0.5}(Na_{0.80}K_{0.20})_{0.5}TiO_3$ (BNKT) thin films were fabricated on the Pt/Ti/SiO_2/Si substrates using the solutions prepared by the sol–gel technique. Here, the BNKT precursor solution was derived from sodium nitrate ($NaNO_3$, ≥99%, Sigma–Aldrich), potassium nitrate (KNO_3, ≥99%, Sigma–Aldrich), bismuth nitrate ($Bi(NO_3)_3 \cdot 5H_2O$, ≥98%, Sigma–Aldrich), and titanium isopropoxide (Ti [i-OPr]$_4$, ≥99%, Sigma–Aldrich). Acetic acid (CH_3COOH) and 2-ethoxyethanol ($CH_3OCH_2CH_2OH$) were chosen as cosolvents. Afterward, 9 mol.% excess amount of potassium nitrate and 11 mol.% excess amount of sodium nitrate were added in order to compensate for the possible loss during the high-temperature annealing. Each layer of the BNKT films was formed by spin coating the 0.4 M yellow precursor solution on the Pt/Ti/SiO_2/Si substrate at 4000 rpm for 30 s, drying at 150 °C for 5 min, followed by pyrolysis at 400 °C for 10 min. The process was repeated until the BNKT thin films with the required coating layers were obtained. Finally, thermal annealing in a high-temperature furnace at different temperatures of 600 °C, 650 °C, 700 °C, 750 °C for 60 min each was carried out to obtain the ferroelectric phase in the BNKT thin films (denoted as S600, S650, S700, S750, respectively). The heating rate in the annealing procedure was 5 °C/min under normal conditions.

Characteristics of the films, including the cross-sectional and the surface morphologies were detected in a field emission scanning electron microscope (FE-SEM, Hitachi S4800) and in an atomic force microscope (AFM, Bruker Dimension ICON). The crystal structures of the BNKT thin films were determined by a Bruker D5005 Diffractometer using Cu-Kα cathode ($\lambda = 1.5406$ Å). Polarization electric field (P–E) hysteresis loops were measured under the applied voltages ranging from −25 V to 25 V, and the frequency of 1000 Hz by using a TF Analyzer 2000 ferroelectric tester (aixACCT Systems GmbH, Germany).

3. Results and discussion

After the heat treatment of the samples, the XRD analyses were carried out to detect the crystal structure and the phase composition of the BNKT films. Fig. 1 (a) shows the XRD patterns of the BNKT films in the 2θ scan range of 28°–62°. All the films show to be of a single-phase composition, indicating that the starting chemicals were completely reacted to form the desired end compounds. The (111) peak with the intensity surpassing that of all others, is characteristic for the Pt-coated substrate. Other peaks, such as (110), (200) and (211) are assigned to the perovskite structure. This result matches previous studies, which proved that the BNKT films with the Kalium concentration of $x = 0.2$ are of both tetragonal and rhombohedral symmetry [18,20,21]. Fig. 1 (b) presents the X-ray diffraction patterns in the 2θ range of 39°–48° for all annealed films. The result shows that the (200) preferred orientations in all the films appear with different intensities. For the sample annealed at 600 °C (S600), the (200) peak is broad and its intensity is low, proving that this sample is not perfectly crystallized. This may stem from the existence of the intermediate pyrochlore phase in the

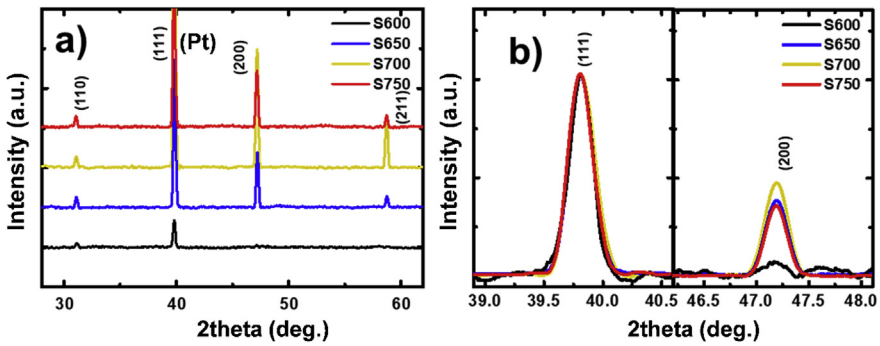

Fig. 1. (a) X-ray diffraction patterns of BNKT films in the 2θ ranges of 28°–62° and (b) X-ray diffraction patterns in the 2θ ranges of 39°–48°.

BNKT film denoted as S600. Chen *et al*. also observed the presence of $Bi_2Ti_2O_7$ pyrochlore phase in the BNKT samples annealed at 550 °C [22]. This pyrochlore phase can be completely changed into the perovskite phase at a higher annealing temperature. With the annealing crystallization temperature increased, the XRD patterns show narrower and sharpener peaks with higher intensities. The intensity of the (200) peak increases significantly and reaches the highest value at 700 °C, before decreasing in the sample annealed at 750 °C. This proved that the BNKT materials were well crystallized at the annealing temperature of 700 °C and the intermediate pyrochlore phase was completely transformed into the perovskite phase [22,23].

Additionally, the enhanced crystallization in the BNKT films also indicates that the grain size is enlarged with the increase of the annealing temperature. The grain size of the BNKT films was calculated for the (200) preferred orientations by using the Scherrer equation [24] below

$$D = \frac{K.\lambda}{\beta.cos\theta} \quad (1)$$

where D is the grain size, K is a constant related to the crystallite shape, (normally taken as 0.9), λ is wavelength, β is the FWHM, and θ is the Bragg angle. Table 1 presents the grain size in the BNKT films as a function of the annealing temperature. Obviously, the value of D increased significantly from 45.3 nm to 49.0 nm when the annealing temperature was raised from 600 °C to 750 °C. Won *et al*. obtained a similar result when investigating the effect of annealing temperature on the properties of $Bi_{0.5}(Na_{0.85}K_{0.15})_{0.5}TiO_3$ thin films [25].

Table 1
The grain size (D), roots mean square roughness (RQ), the maximum polarization (P_m), remnant polarization (P_r), difference between P_m and P_r (P_m - P_r), the coercive field (E_C) the energy storage density (J_{reco}), energy loss density (J_{loss}) and energy storage efficiency (η) as a function of the annealing temperature.

Annealing temperature (°C)	600	650	700	750
D (nm)	45.3	46.5	48.9	49.0
RQ (nm)	4.8	4.6	4.5	3.4
P_r (μC/cm^2)	6.86	6.88	9.17	6.37
P_m (μC/cm^2)	13.72	20.64	30.57	21.40
$P_m - P_r$ (μC/cm^2)	6.86	13.76	21.40	15.03
E_C (kV/cm)	115.0	85.1	78.5	78.4
J_{reco} (J/cm^3)	0.62	1.68	2.33	1.72
J_{loss} (J/cm^3)	1.17	1.21	1.78	1.25
η (%)	34.7	58.2	56.7	57.9

2*D*-3*D* AFM images of the BNKT films prepared at different annealing temperatures are shown in Fig. 2 (*a*)–(*d*). With the scanning area of 40 μm × 40 μm, all AFM images show the smooth surface morphologies and no cracks are detected. Surface cracks, stemming from the film stress, cause a dielectric loss in the films. Another important parameter contributing to the quality of device applications is the surface roughness of the films. A good interface between the film and the metal substrate requires a smooth and defect-free surface morphology. The surface roughness of the film is evaluated through the root-mean-square (RQ) approach, which was calculated automatically by using the AFM equipment's routine software. The RQ values of the films ranging from 3.4 nm to 4.8 nm are also shown in Table 1. The RQ has such a small value, confirming that BNKT films exhibit good surface quality. The well-distributed grains and good surface quality of the films will be reliable bases to improve the ferroelectricity. Fig. 2 (*e*) and (*f*) show the FE-SEM micrograph and the cross-sectional SEM image of the S700 sample, respectively. The images show that the films are homogenous and fairly dense. The thicknesses of the films were determined from cross-sectional FE-SEM images and Fig. 2 (*f*) shows the thickness of the films to be of approximately 300 nm.

Fig. 3 (*a*) shows the polarization (*P*–*E*) hysteresis loops for the BNKT films annealed at different temperatures. Generally, all the films exhibit the same form of *P*-*E* hysteresis loops, characteristic for the ferroelectric materials. The films annealed at different temperatures exhibit variations in the values of $2P_m$, $2P_r$, $2(P_m - P_r)$ and E_C. With an increase in the crystallization temperature from

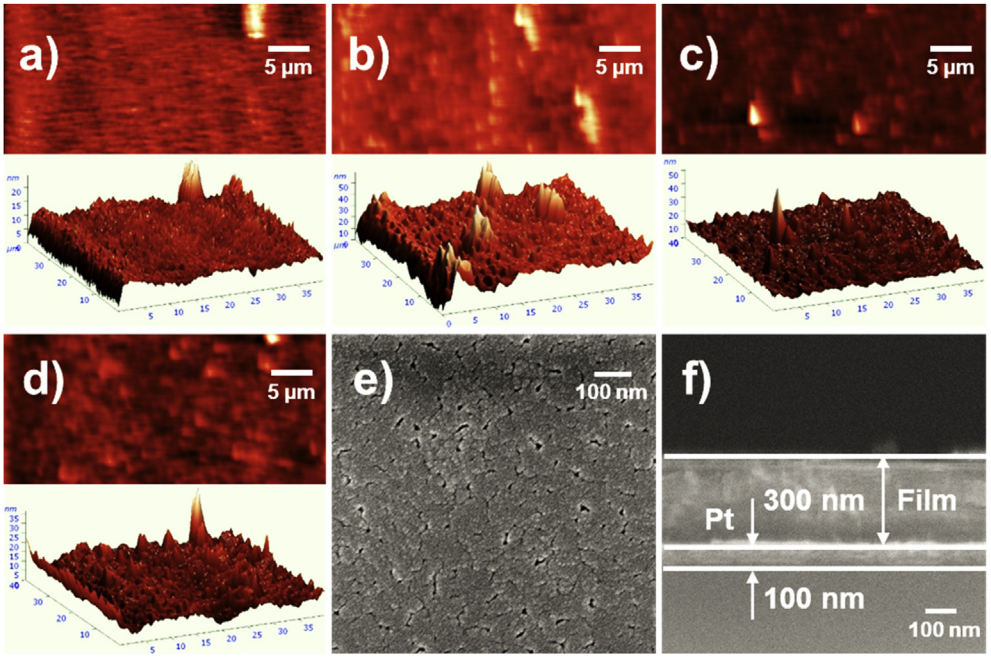

Fig. 2. 2D - 3D AFM images of BNKT films at different crystallization temperatures: (a) S600, (b) S650, (c) S700, (d) S750; (e) FE-SEM micrographs of sample S700 and (f) Cross-sectional SEM image of sample S700.

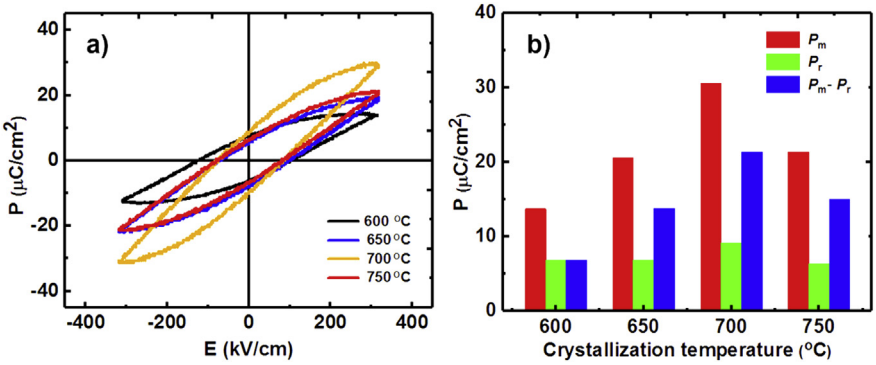

Fig. 3. (a) *P–E* ferroelectric hysteresis loops, (b) The maximum polarization (P_m), the remnant polarization (P_r), the difference between P_m and P_r (P_m - P_r) of BNKT films annealed at different temperatures with the same applied electric field of 300 kV/cm.

600 °C to 750 °C, the coercive field decreases and reaches a minimum value of 78 kV/cm. This stems from the larger deformations in the lattice, facilitating the domain movement. The energy barrier for switching the ferroelectric domains decreases as the grain size increases, causing the repulsive force between neighboring domain walls to decline; hence, the ferroelectric films need a lower activation energy for the reorientation of the domains. Fig. 3 (*b*) shows the maximum polarization (P_m), the remnant polarization (P_r), the difference between P_m and P_r (P_m - P_r) of the BNKT films annealed at different temperatures. In the S600 films, $2P_m$ and $2P_r$ have relatively low values of around 27.4 μC/cm^2 and 13.8 μC/cm^2, respectively. The difference between the values of $2P_m$ and $2P_r$ is 13.6 μC/cm^2. But, $2P_m$ and $2P_r$ are significantly enhanced when the crystallization temperature increases from 600 °C to 700 °C. The thin film annealed at 700 °C shows the $2P_r$ and $2P_m$ values of 18.4 μC/cm^2 and 61.2 μC/cm^2, respectively, and the difference between the values of $2P_m$ and $2P_r$ is 42.8 μC/cm^2, all of which are significantly larger than those of the S600 film. However, the film obtained at the crystallization temperature of 750 °C exhibits a decline in $2P_r$ and $2P_m$. The effect of the annealing temperature on $2P_r$ and $2P_m$ can be unraveled as follows. The grain boundary region has a low-permittivity, *i.e.* it possesses weak ferroelectricity. Hence, the polarization of the grain boundary may be little, and even diminishes. Additionally, the grain boundary possesses space charges, which exclude the polarization charge on the grain surface, thus, forming a depletion layer on the grain surface. This depletion layer causes the polarization discontinuity at the grain surface, forming a depolarization field, causin a decrease of polarization. When the annealing temperature is increased from 600 °C to 750 °C, the grains in the BNKT films merge, becoming bigger and hence the ratio of grain boundary to grain core volume decreases. Thus, no sooner the grain size increases than the $2P_r$ and $2P_m$ also rise. Because of the inherent hysteresis in the ferroelectric materials, the energy delivered to the capacitors can not discharge completely. Hence, the energy storage density (J_{reco}), the energy loss density (J_{loss}) and the energy storage efficiency (η), which are important parameters for energy storage applications, should be carefully taken into consideration. The J_{reco}, J_{loss}, and η are calculated by using equations (2)–(4), respectively [26]:

$$J_{reco} = \int_{P_r}^{P_m} EdP \tag{2}$$

$$J_{loss} = \int_{0}^{P_m} EdP - J_{reco} \tag{3}$$

$$\eta = \frac{J_{reco}}{J_{reco} + J_{loss}} \times 100 \tag{4}$$

where E refers to the applied electric field; P_m and P_r are the maximum and remnant polarization values, respectively. The schematic diagram for the calculation of the energy storage properties of ferroelectric films are demonstrated in Fig. 4 (*a*). J_{reco} is the electrical energy density stored in the material, obtained by integrating the *P-E* hysteresis loops along the discharging curve. J_{loss} is the energy corresponding to the inherent hysteresis in the material. It is obtained by integrating the area between the charge and discharge curve.

Fig. 4 (*b*) exposes the energy storage density (J_{reco}), the energy loss density (J_{loss}) and the energy storage efficiency (η) of the BNKT films as a function of the crystallization temperature at the applied electric field E_{appl} of 300 kV/cm. It can be seen that J_{reco} and η show the same changing tendency and increase with the rise of crystallization temperature. BNKT films annealed at the 600 °C exhibit J_{reco} and η values as low as 0.6 J/cm^3 and 34.7%, respectively. These parameters reach their highest values of about 2.3 J/cm^3 and 58.2%, respectively. However, J_{reco} gets its maximum value with the annealing temperature of 700 °C, while η with 650 °C, respectively. According to equations (2)–(4), the enhancement in J_{reco} and η are contributed by the following factors: *i*) the value of the breakdown strength (BDS) and *ii*) the polarization difference (P_m - P_r) [27]. The grain size has a strong influence on the BDS of ferroelectric materials. Tunkasiri *et al.* reported that the BDS is closely related to the grain size of the ferroelectric materials, based on the expression [28]:

$$E_B \sim 1/\sqrt{D} \tag{5}$$

where E_B and D are the electric fields corresponding to the BDS of materials and the grain size, respectively. Equation. (5) shows that the increase in grain size causes the BDS of materials to decrease. When the annealing temperature rises, the grain size also increases (Table 1), followed by a decrease of BDS. This leads to a decrease of J_{reco}. In contrast, P_m - P_r value exhibits an increasing trend, contributing to the enhancement of the energy-storage properties.

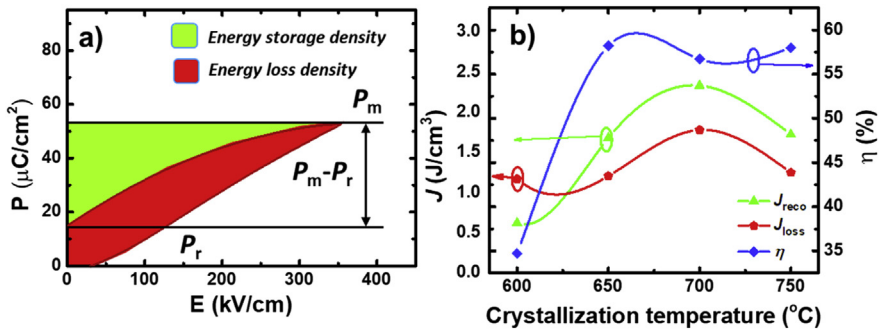

Fig. 4. (a) Schematic diagram for the calculation of energy storage properties of ferroelectric films, (b) Energy storage density, energy loss density and energy storage efficiency as a function of the crystallization temperature.

Because of the combination of the two opposite factors, J_{reco} and η reach their highest values at different temperatures.

Compared to previous reports, J_{reco} and η values in this study surpass those of bulk ceramics. Xu and his co-workers [29] obtained the solid solubility of BNTBT with NBN and optimized the energy-storage properties with $J_{reco} = 1.36$ J/cm^3 and $\eta = 73.9\%$ at NBN content of 0.02. By La and Zr co-doping, Lu and his co-workers [30] enhanced the energy-storage capacity of the BNTBT (the maximum J_{reco} was 1.21 J/cm^3 at 100 kV/cm). In the report [31], the influence of KN addition on the energy storage density of BNBT–xKN ceramics was discussed. It was found that BNBT–0.06 KN exhibits the highest J_{reco} value of 0.89 J/cm^3 at 100 kV/cm whereas the $(1 - x)$BNTBT-xNN ceramics [32] show (narrower) P–E loops with the increasing NN amount. Therefore, the J_{reco} was enhanced significantly and reached the highest value of 0.71 J/cm^3 for $x = 0.10$ at 7 kV/mm. Cao and his co-workers [33] found 0.7NBT-0.3ST possessing excellent temperature stability in the range from the room temperature to 120 °C and the maximum J_{reco} value of 0.65 J/cm^3 at 65 kV/cm. However, our results show poorer energy-storage properties than those previously reported on BNKT films. NBT films [34] on LNO/Si (100) substrates exhibit good energy-storage properties at 1200 kV/cm ($J_{reco} = 12.4$ J/cm^3 and $\eta = 43\%$). Zhang and his co-workers [35] when substituting Ti^{4+} by Mn^{2+}, markedly improved the energy-storage properties of 0.7NBT-0.3ST films. With Mn-dopant concentration of 1 mol. %, the BDS value was raised to 1894 kV/cm, resulting in the enhanced J_{reco} value of 27 J/cm^3. The discrepancy of these values to ours appear because our study was only conducted on BNKT-pure films and focused on improving the processing conditions.

4. Conclusion

Lead-free $Bi_{0.5}(Na_{0.8}K_{0.2})_{0.5}TiO_3$ (BNKT) films have been successfully prepared on Pt/Ti/SiO_2/Si substrates via a spin coating assisted sol–gel routine. The properties of the films, such as the microstructures, ferroelectricity and energy-storage behavior were investigated as a function of the crystallization temperature. All film samples have a smooth and crack-free surface morphology and a single-phase composition with the defined perovskite structure. The investigations revealed the optimal crystallization temperature of 700 °C for the materials of interest. At this, $2P_r$ and $2P_m$ reached their peak values of 18.4 μC/cm^2 and 61.2 μC/cm^2, respectively. The enhancement of the ferroelectric properties originate from: i) the increase of the grain size; ii) the complete transformation of the intermediate pyrochlore phase into the perovskite phase. Besides, higher P_m - P_r were achieved for the film annealed at 700 °C. As a result, J_{reco} and η reach the highest values of 2.3 J/cm^3 and 58.2%, respectively. Obtained results suggest that the BNKT films can be considered as a promising alternative energy storage application.

Acknowledgements

This research is funded by Vietnam National Foundation for Science and Technology Development (NAFOSTED) under grant number 103.02-2017.21.

References

[1] W. Jo, R. Dittmer, M. Acosta, J. Zang, C. Groh, E. Sapper, K. Wang, J. Rödel, Giant electric-field-induced strains in lead-free ceramics for actuator applications – status and perspective, J. Electroceram. 29 (2012) 71–93.
[2] N.D. Quan, L. Huu Bac, D.V. Thiet, V.N. Hung, D.D. Dung, Current development in lead-free $Bi_{0.5}(Na,K)_{0.5}TiO_3$-based piezoelectric materials, Adv. Mater. Sci. Eng. 2014 (2014) 1–13.
[3] G.O. Jones, J. Kreisel, P.A. Thomas, An investigation of the crystal structures in the $(Na_xK_{1-x})_{0.5}Bi_{0.5}TiO_3$ series, Powder Diffr. 17 (2002) 301–319.
[4] J. Kreisel, A.M. Glazer, G. Jones, P.A. Thomas, L. Abello, G. Lucazeau, An x-ray diffraction and Raman spectroscopy investigation of A-site substituted perovskite compounds: the $(Na_{1-x}K_x)_{0.5}Bi_{0.5}TiO_3$ ($0 < x < 1$) solid solution, J. Phys. Condens. Matter 12 (2000) 3267.
[5] A. Sasaki, T. Chiba, Y. Mamiya, E. Otsuki, Dielectric and piezoelectric properties of $(Bi_{0.5}Na_{0.5})TiO_3$–$(Bi_{0.5}K_{0.5})TiO_3$ systems, Jpn. J. Appl. Phys. 38 (1999) 5564.
[6] O. Elkechai, M. Manier, J.P. Mercurio, $Na_{0.5}Bi_{0.5}TiO_3$–$K_{0.5}Bi_{0.5}TiO_3$ (NBT-KBT) system: a structural and electrical study, Phys. Status Solidi 157 (1996) 499–506, https://doi.org/10.1002/pssa.2211570234.
[7] R.E. Eitel, A.R. Clive, R.S. Thomas, W.R. Paul, H. Wes, P. Seung-Eek, New high temperature morphotropic phase boundary piezoelectrics based on Bi(Me)O_3–$PbTiO_3$ ceramics, Jpn. J. Appl. Phys. 40 (2001) 5999.
[8] H. Yuji, W. Tomomi, N. Hajime, T. Tadashi, Piezoelectric properties of $(Bi_{1/2}Na_{1/2})TiO_3$-based solid solution for lead-free high-power applications, Jpn. J. Appl. Phys. 47 (2008) 7659.
[9] M. Otoničar, S.D. Škapin, M. Spreitzer, D. Suvorov, Compositional range and electrical properties of the morphotropic phase boundary in the $Na_{0.5}Bi_{0.5}$-TiO_3–$K_{0.5}Bi_{0.5}TiO_3$ system, J. Eur. Ceram. Soc. 30 (2010) 971–979.
[10] P. Tang, K. Yu, X. Xie, S. Zhou, J. Yao, Research on the excitation control of brushless doubly-fed alternator in a novel pulse capacitor charge power supply, IEEE Trans. Plasma Sci. 45 (2017) 1288–1294, https://doi.org/10.1109/TPS.2017.2705153.
[11] D. Fu, F.C. Lee, Y. Qiu, F. Wang, A novel high-power-density three-level LCC resonant converter with constant-power-factor-control for charging applications, IEEE Trans. Power Electron. 23 (2008) 2411–2420.
[12] L. Zhang, X. Ren, Aging behavior in single-domain Mn-doped $BaTiO_3$ crystals: implication for a unified microscopic explanation of ferroelectric aging, Phys. Rev. B 73 (2006) 094121, https://doi.org/10.1103/PhysRevB.73.094121.
[13] W. Cao, W. Li, Y. Feng, T. Bai, Y. Qiao, Y. Hou, T. Zhang, Y. Yu, W. Fei, Defect dipole induced large recoverable strain and high energy-storage density in lead-free $Na_{0.5}Bi_{0.5}TiO_3$-based systems, Appl. Phys. Lett. 108 (2016) 202902.
[14] J. Huang, Y. Zhang, T. Ma, H. Li, L. Zhang, Correlation between dielectric breakdown strength and interface polarization in barium strontium titanate glass ceramics, Appl. Phys. Lett. 96 (2010) 042902, https://doi.org/10.1063/1.3293456, 2902.
[15] Y. Wu, X. Wang, C. Zhong, L. Li, Effect of Mn doping on microstructure and electrical properties of the $(Na_{0.85}K_{0.15})_{0.5}Bi_{0.5}TiO_3$ thin films prepared by sol–gel method", J. Am. Ceram. Soc. 94 (2011) 3877–3882.
[16] M. Budimir, D. Damjanovic, N. Setter, Enhancement of the piezoelectric response of tetragonal perovskite single crystals by uniaxial stress applied along the polar axis: a free-energy approach, Phys. Rev. B 72 (2005) 064107, https://doi.org/10.1103/PhysRevB.72.064107.
[17] N.D. Quan, T.Q. Toan, V.N. Hung, Influence of crystallization time on energy-storage density and efficiency of lead-free $Bi_{0.5}(Na_{0.8}K_{0.2})_{0.5}TiO_3$ thin films, Adv. Condens. Matter Phys. 2019 (2019) 1–8.

[18] N.D. Quan, V.N. Hung, D.D. Dung, Influence of film thickness on ferroelectric properties and leakage current density in lead-free $Bi_{0.5}(Na_{0.80}K_{0.20})_{0.5}TiO_3$ films, Mater. Res. Express 4 (2017) 086401.
[19] N.D. Quan, N.V. Hong, T.Q. Toan, V.N. Hung, Enhanced ferroelectric properties and energy storage density in PLZT/BNKT heterolayered thin films prepared by sol–gel method, Eur. Phys. J. B. 91 (2018) 316.
[20] N.D. Quan, V.N. Hung, D.D. Dung, Effect of Zr doping on structural and ferroelectric properties of lead-free $Bi_{0.5}(Na_{0.80}K_{0.20})_{0.5}TiO_3$ films, J. Electron. Mater. 46 (2017) 5814–5819, https://doi.org/10.1007/s11664-017-5603-9.
[21] N.D. Quan, V.N. Hung, I.W. Kim, D.D. Dung, Bipolar electric field induced strain in Li substituted lead-free $Bi_{0.5}(Na_{0.82}K_{0.18})_{0.5}Ti_{0.95}Sn_{0.05}O_3$ piezoelectric ceramics, J. Nanosci. Nanotechnol. 16 (2016) 7978–7982.
[22] P. Chen, S. Wu, P. Li, J. Zhai, B. Shen, The phase formation process of $Bi_{0.5}(Na_{0.8}K_{0.2})_{0.5}TiO_3$ thin films prepared using the sol-gel method, Ceram. Int. 44 (2018) 6402–6408.
[23] N.D. Quan, T.Q. Toan, V.N. Hung, M.-D. Nguyen, Influence of crystallization temperature on structural, ferroelectric and ferromagnetic properties of lead-free $Bi_{0.5}(Na_{0.8}K_{0.2})_{0.5}TiO_3$ multiferroic films, Adv. Mater. Sci. Eng. 2019 (2019) 1–10.
[24] A. Monshi, M.R. Foroughi, M.R. Monshi, Modified scherrer equation to estimate more accurately nano-crystallite size using XRD, World J. Nano Sci. Eng. 02 (2012) 154–160.
[25] S.S. Won, C.W. Ahn, I.W. Kim, The effect of annealing temperature on the piezoelectric and dielectric properties of lead-free $Bi_{0.5}(Na_{0.85}K_{0.15})_{0.5}TiO_3$ thin films, J. Korean Phys. Soc. 61 (2012) 928–932.
[26] H. Borkar, V.N. Singh, B.P. Singh, M. Tomar, V. Gupta, A. Kumar, Room temperature lead-free relaxor–antiferroelectric electroceramics for energy storage applications, RSC Adv. 4 (2014) 22840–22847.
[27] Z. Sun, L. Li, S. Yu, X. Kang, S. Chen, Energy storage properties and relaxor behavior of lead-free $Ba_{1-x}Sm_{2x/3}Zr_{0.15}Ti_{0.85}O_3$ ceramics, Dalton Trans. 46 (2017) 14341–14347.
[28] T. TUNKASIRI, G. RUJIJANAGUL, Dielectric strength of fine grained barium titanate ceramics, J. Mater. Sci. Lett. 15 (1996) 1767–1769.
[29] Q. Xu, H. Liu, Z. Song, X. Huang, A. Ullah, L. Zhang, J. Xie, H. Hao, M. Cao, Z. Yao, A new energy-storage ceramic system based on $Bi_{0.5}Na_{0.5}TiO_3$ ternary solid solution, J. Mater. Sci. Mater. Electron. 27 (2015) 322–329.
[30] X. Lu, J. Xu, L. Yang, C. Zhou, Y. Zhao, C. Yuan, Q. Li, G. Chen, H. Wang, Energy storage properties of $(Bi_{0.5}Na_{0.5})_{0.93}Ba_{0.07}TiO_3$ lead-free ceramics modified by La and Zr co-doping, J. Materiomics 2 (2016) 87–93.
[31] B. Wang, L. Luo, X. Jiang, W. Li, H. Chen, Energy-storage properties of $(1-x)Bi_{0.47}Na_{0.47}Ba_{0.06}TiO_{3-x}KNbO_3$ lead-free ceramics, J. Alloy. Comp. 585 (2014) 14–18.
[32] Q. Xu, T. Li, H. Hao, S. Zhang, Z. Wang, M. Cao, Z. Yao, H. Liu, Enhanced energy storage properties of $NaNbO_3$ modified $Bi_{0.5}Na_{0.5}TiO_3$ based ceramics, J. Eur. Ceram. Soc. 35 (2015) 545–553.
[33] W.P. Cao, W.L. Li, X.F. Dai, T.D. Zhang, J. Sheng, Y.F. Hou, W.D. Fei, Large electrocaloric response and high energy-storage properties over a broad temperature range in lead-free NBT-ST ceramics, J. Eur. Ceram. Soc. 36 (2016) 593–600.
[34] Y. Zhao, X. Hao, M. Li, Dielectric properties and energy-storage performance of $(Na_{0.5}Bi_{0.5})TiO_3$ thick films, J. Alloy. Comp. 601 (2014) 112–115.
[35] Y. Zhang, W. Li, W. Cao, Y. Feng, Y. Qiao, T. Zhang, W. Fei, Mn doping to enhance energy storage performance of lead-free 0.7NBT-0.3ST thin films with weak oxygen vacancies, Appl. Phys. Lett. 110 (2017) 243901.